EXPERIMENTAL COMPARISON OF INFRARED THERMOGRAPHY, HOLOGRAPHIC INTERFEROMETRY AND ACOUSTO - ULTRASONICS ON A COMPLEX SANDWICH STRUCTURE SAMPLE

S. Sfarra[1], A. Bendada[2], C. Ibarra-Castanedo[2], N.P. Avdelidis[3], T.H. Loutas[4], G. Sotiriadis[4], V. Kostopoulos[4], D. Ambrosini[1], D. Paoletti[1], X. Maldague[2]

[1]Las.E.R. Laboratory, DIMEG, University of L'Aquila, Italy
[2]Department of Electrical Engineering, Laval University, Quebec City, Canada
[3]School of Chemical Engineering, National Technical University of Athens (NTUA), Greece
[4]Department of Mechanical & Aeronautical Engineering, University of Patras, Greece

1. Introduction

World-wide interest on the use of ceramic coatings as key load-bearing components for gas turbine, aerospace and other advanced engineering applications, has led to the need for inspection techniques capable of detecting unusually small structural anomalies in these components.
Modern ceramic materials offer many attractive physical and mechanical properties for a wide and rapidly growing range of industrial applications; moreover specific use may be made of their wear resistance, chemical resistance, and thermal barrier properties [1].
A major drawback with these materials is the catastrophic nature with which they fail once their critical stress level is reached; flaws can be introduced in ceramic coating during the manufacturing process or in service conditions.
In order to examine the quality of a coating it is necessary to know its function. For instance, coatings intended for decorative purposes have to meet different requirements from those serving as protection against wear and temperature.
As a basis for the quality of a coating, many different factors are of importance, such as coating thickness, adhesive strength, residual stresses, coating flaws (bonding flaws, cracks, inclusions), ductility or also tribological properties.
Increasingly, non-destructive testing (NDT) is being used to evaluate the coating thickness and to test the coating for flaws. The main advantage of NDT is the intact state of the object after testing and thus the possibility to continue its usage.
The definition of "flaw" comprises both production-induced and operationally caused changes of properties. Particularly in the case of testing heavily stressed components, e.g. in the aerospace industry, a high safety standard is assured by non-destructive inspection only. This procedure offers a guarantee for early detection and evaluation of operationally caused damage and with that the prerequisite for estimating possible failure and lifetime of the components.
Also, the sandwich materials are subject to different defects both in phase of production and in service conditions. A sandwich structure composite is a special class of composite materials that is fabricated by attaching two thin but stiff skins to a lightweight but thick core. The core material is normally low strength material, but its higher thickness provides the sandwich composite with high bending stiffness with overall low density. The main benefits of using the sandwich concept in structural components are the high stiffness, the good fatigue resistance and the low weight. Recent advances in materials and manufacturing techniques have resulted in further improvements and in an increased uniformity of the properties of sandwich composites.
Alumina components, like the one is being use for the top layer of our complex sandwich structure sample is constituted and that it intends to simulate a "coating", have recently been used in the manufacture of a new material called AETB-8 (Alumina Enhanced Thermal Barrier). The addition of small quantities of Al_2O_3, increases the thermal stability and the conductivity without a meaningful increase of weight or diminution of resistance.

The sticking by an adhesive tape of the sandwich structure with simulated defects and the alumina tile with a real defect, it is also arose from an idea to detect a complex structure through three different non-destructive techniques - infrared thermography (IRT), holographic interferometry (HI) and acousto ultrasonics (AU), with the purpose to confirm by this integration process every single defectiveness found. Both these materials, were furnished by the Thales Alenia Space, are used in the spatial sector.
Space structures are exposed to severe in-service conditions. In order to receive a high safety of operation, possible damages must be recognized prematurely within control examinations to prevent the total breakdown of the component.
Consequently, non-destructive testing (NDT) is a vital process to ensure structural integrity; the investigation with respect to material and construction imperfections is of high interest. Due to the diversity and complexity of space components, the modern test engineer must become skilled in several complementary inspection methods.
Optical and Thermal NDT are two areas that are likely to experience increasing interest for the inspection of composite materials. They offer several advantages over conventional inspection and many of the technical problems that have prevented their industrialization in the past have now been overcome.
Besides, AU, a highly sophisticated and advanced technique using digital signal processing and pattern recognition algorithms, assures a further confirmation in the individualization of the found defects.

2. Generality and constructive details of the complex sandwich structure sample

The sample (102 x 102 x 7 mm) on which our analyses have been effected is reported in Figure 1. The materials that constitute the specimen, provided by Thales Alenia Space, consists of a carbon fiber honeycomb core between two CFRP layers (0, 90) skins (thickness = 6 mm), bonded in a side by double sided adhesive tape with a ceramic plate in alumina (thickness = 1 mm).
The adhesive utilized for the sandwich structure was the AF191U thickened with air warm neighbour the cell wall. The specimen core was pierced from the side 1 (defects A and C as seen in Figures 1b and 1c) in our laboratories. The fabricated holes have the same diameter (φ = 5 mm), and size (L = 70 mm), and were pierced to the same depth (z = 0.5 mm). Both the holes have been filled with two sponges covered by Teflon with the purpose to simulate some inclusions. Another fabricated defect has been realized on the side 2 (defect D as seen in Figures 1a and 1b). A portion of honeycomb has been removed (10 x 11 x 6 mm) with the intent to simulate a loss of material after an impact.
By HI method – Real Time technique (RT) –, has been possible to identify the presence of the defect B (as seen in Figure 1b) inherent the ceramic material, due probably or to the thermal shocks which the sample has been subjected or to a not correct process of manufacture.

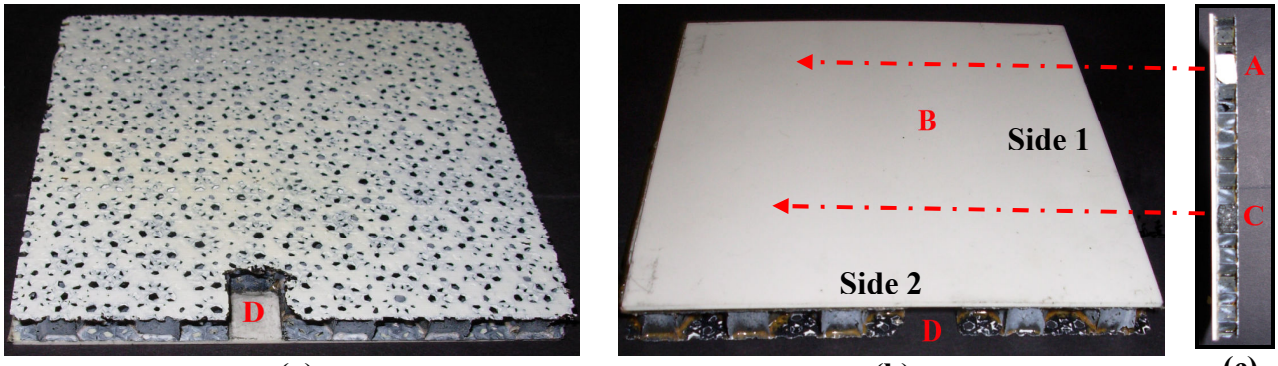

(a) **(b)** **(c)**

Figure 1.(a) Rear part of the complex sample showing the sandwich structure, (b) top part of the complex sample showing the alumina ceramic plate, the location of defect B and the fabricated defect D in side 2, (c) lateral view of the complex sandwich structure sample showing the cross-section of the fabricated defects A and C.

The name “complex sandwich structure sample” is due to the assemblage of three layers:

- *substratum in alumina to thin film (99.6%)*, (Figure 1b) whose fundamental characteristics are: good thermal stability, is not subject to the oxidation, excellent hardness (similar to the diamond), the alumina has a Vickers hardness of 1600 MPa in comparison to that of a rapid steel that is of 900 MPa; excellent usury resistance - the life time of a ceramic component in the applications under usury is greater to that of the same steel component of 10 - 14; corrosion resistance in acid or alkaline environments; good electric insulator - excellent dielectric property from direct current to the frequencies of the GHz; good thermal insulator; high specific area - in the porous microform or nanoporous reaches areas of 300 m^2/g; excellent biocompatibility. However, the alumina also has a not elevated mechanical resistance and low resistance to the thermal shocks. [2, 3].
- *Double sided adhesive tape*, (Figure 1c) with the purpose to simulate the pasting between the honeycomb and the ceramic tile.
- *Sandwich structure,* (Figure 1a) this honeycomb part was originally used for an antenna reflector for a spacecraft. In one embodiment, the antenna reflector comprises at least one outer layer of an electrically conductive and electrically reflective material including a plurality of openings formed therein. The antenna reflector also comprises at least one inner layer of a fabric material bonded to the outer layer. The fabric material includes a plurality of openings formed therein. The combination of the openings in the outer layer and the openings in the inner layer allow acoustic noise to be transmitted and dissipated through the openings. Usually this invention is directed to a method of forming a reflector membrane for an antenna reflector for a spacecraft. In one embodiment, the method includes forming at least one outer layer of an electrically conductive and electrically material including several openings formed therein. An inner layer is formed of a fabric material, the fabric material including a plurality of openings therein. The openings of the outer layer are aligned with the openings of the inner layer to form a plurality of combined openings in the reflector membrane. The combined openings are adapted to allow acoustic noise transmission and dissipation through the combined openings. The antenna reflector is adapted to operate in at least a microwave frequency band. The outer layer is bonded to the inner layer. In a further aspect, the present invention is directed to an antenna reflector structure for reflecting microwaves emitted and received by a microwave antenna while operating in space. In one embodiment, the antenna reflector structure comprises, in combination, the elements of a first surface microwave reflective mesh layer affixed to a second tri-axial women fabric structural layer, the second layer having holes formed within the fabric by the intersection of three fibers oriented tri-axially in three directions to one another. The first microwave reflective layer is a mesh having holes or openings that are large enough to allow acoustic noise waves produced during launch of the antenna on a spacecraft into space to be transmitted through the holes in the reflective mesh layer and through the holes that exist in the second tri-axial women fabric layer. The holes in the first microwave reflective mesh layer are small enough to still reflect the microwaves [4].

3. Holographic Interferometry (HI)

Holographic Interferometry produces interference between two or more waves, at least one of which is reconstructed by a hologram. The interfering waves may be separated in time. Holographic Interferometry allows measurements, inspection and testing of not only optically flat surfaces but also of any three dimensional surface of arbitrary shape. It also allows interferometric examination of the object in different perspectives.

Conventional optical interferometry can be used for optically polished and specularly reflecting surfaces only. If the object is considered to be made up of small mirror elements, then a single holographic interferogram can be equivalent to a large number of observations from a conventional optical interferometry.

The object wavefront can be stored in a hologram and compared with the object after a change that may have taken place. It is this storage or time delay aspect which gives the holographic method a unique advantage over conventional optical interferometry.
Horman [5] was the first to suggest the application of a hologram in the test arm of a Mach-Zehnder interferometer.
The holographic interferometry of 3D objects was first introduced by Powell and Stetson [6] almost simultaneously.
In general, three forms of holographic interferometry are possible viz. double-exposure, single exposure real time and sandwich holography.
Originally, however, each of these techniques required a specific arrangement of optical components, depending on what was to be tested and how it was to be loaded or stressed in order to locate a flaw or debond [7].

3.1 Real Time (RT) Holographic Interferometry

In double-exposure technique the object can be studied at two fixed stressing conditions only unless multiplexing technique are used to study the intermediate conditions. However, in many applications it is desirable to see the response of the object to a series of excitations. This can be accomplished by single-exposure real-time holographic interferometry which is also known as concomitant or live-fringe interferometry.
A single-exposure hologram of the object is recorded. The photographic plate is either developed in situ or removed from the setup, processed, dried and repositioned in its original recording position. The hologram is reconstructed by the reference beam. An observed looking through the hologram will see the virtual image of the object superimposed on the actual object which is still being illuminated by the laser beam. If the reconstruction has been done properly, the null condition results.
If the object is now deformed, the observer will see the object superimposed with interference fringes which are produced due to interference between the reconstructed wave and the object wave.
The fringe pattern will change in real time if the object is subjected to different amount of stresses or deformations. The fringes will have a cosinusoidal intensity pattern. A vibrating object can also be studied through Real-Time holographic interferometry. The fringe pattern will be indicative of the vibrational amplitude but the irradiance of the fringes will be weak due to the integrating time of the eye.
The instantaneous irradiance for a real-time hologram is given by:

$$I(x,y,t) = |U_0|^2 2\{1 - \cos[\Delta\phi(x,y,t)]\} \tag{1}$$

The minus sign in Eq. (1) appears because the complex amplitude of the reconstructed object wave is negative due to a uniform phase shift of π rad.
The Real-Time holographic interferometry requires repositioning of the processed hologram with interferometric accuracy.

3.2 Double-Exposure (DE) Holographic Interferometry

In Double-Exposure holographic interferometry, two holograms of the two object waves occurring sequentially in time are recorded on a single photographic plate. When such a hologram is reconstructed. The interference between these images produces interference fringes overlaid on the image of the object. The interference fringes are indicative of deformation, displacement, rotation and change in refractive index or thickness of the object. The fringes appear to be localized in space, not necessarily on the object. When viewing direction is altered, the fringes shift and change their form.

A hologram of the object in its initial unstressed state is recorded by exposing the photographic plate.
Without removing the photographic plate from the setup, the object is stressed and a second exposure is made.
The plate is then developed and reconstructed by the reconstruction wave to observe the interference. Let U_0 (x,y) and U (x,y) represent the complex amplitudes of the object wave before and after stressing and U_r (x,y) the complex amplitude of the reference wave. Then:

$$U_0(x,y) = O_0(x,y)\exp[-j\phi(x,y)] \tag{2}$$
$$U(x,y) = O_0(x,y)\exp\{-j[\phi(x,y)+\Delta\phi(x,y)]\} \tag{3}$$

The stressing introduces a small change in the phase $\Delta\phi(x,y)$. The phase $\phi(x,y)$ is given by:

$$\phi(x,y) = \frac{2\pi nd}{\lambda} \tag{4}$$

Where n is the refractive index of the medium in which the light propagates and d is the physical path length from laser to the recording plate via object.
Both the states of the object are recorded as a Double-Exposure hologram using a reference wave of complex amplitude $U_r(x,y)$.
When the plate is developed and reconstructed by $U_r(x,y)$, the complex amplitude of the reconstructed wave will be proportional to:

$$[U_0(x,y)+U(x,y)]$$

The irradiance of the reconstructed wave will be proportional to:

$$I(x,y) = |U_0(x,y)+U(x,y)|^2 = |O_0(x,y)|^2 \cdot 2\{1+\cos[\Delta\phi(x,y)]\} \tag{5}$$

Eq. (5) indicates that the object irradiance $|O_0(x,y)|^2$ is modulated by the fringe pattern $2\{1+\cos[\Delta\phi(x,y)]\}$.
The change in phase ΔΦ may be related to displacement, rotation, tilt, bending, vibrational amplitude, temperature, pressure, strain, stress, electron density or mass concentration. The fringe represents the locus across the field which is associated with a particular optical path. The distance between two consecutive fringes represents a change equal to a wavelength in the optical path from the first exposure to the second. If no phase changes are induced between the two exposures, the fringes will be nonexistent. Bright fringes are the contours of ΔΦ values which are even-integer multiples of π, whereas the dark fringes correspond to the contours of constant ΔΦ values which are odd-integer multiples of π.
Double-Exposure interferometric technique (DE) is simple to implement as no alignment is involved in the two reconstruction images.
The Double-Exposure technique gives a permanent record of the change in the shape of the object between exposures.
The fringes have good contrast and visibility as distortions in the emulsion and imperfections in the optical components affect both the images equally and the two diffracted wavefronts are similarly polarized.
The intensity of the reconstructed waves can be made equal by controlling the two exposure times to get high contrast fringes [8].
Figure 2 shows the RT and DE configuration.

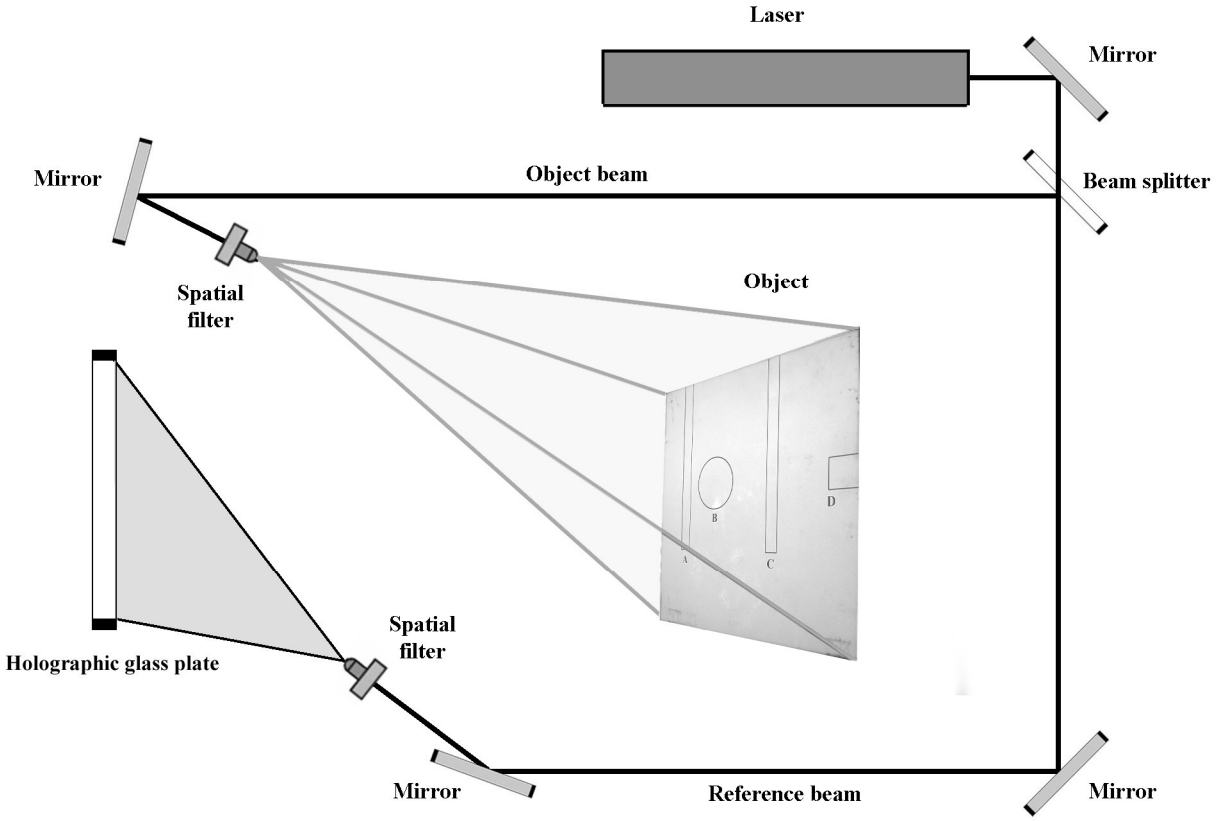

Figure 2. Experimental configuration for Real-Time (RT) and Double-Exposure (DE) HI.

4. Pulsed Thermography (PT)

Infrared thermography (PT) is one of the simplest and fastest NDE techniques that does not require a physical contact with the piece being inspected. IRT is however affected by a variety of problems such as reflections from the environment, emissivity variations, non-uniform heating and surface geometry variation. It is possible to have control over some of these effects. Furthermore, the non-uniformity of the energy source is an unavoidable problem that can only be minimized while carrying out the experiment and/or corrected through processing. Several techniques can reduce the impact of some or all these problems.

4.1 Theory

Heat diffusion through a solid is a complex 3D problem that can be described by Fourier's law of heat diffusion [9]:

$$\nabla^2 T - \frac{1}{\alpha} \cdot \frac{\partial T}{\partial t} = 0 \tag{6}$$

where ∇ is the 3D del operator (in the 3D Cartesian coordinate system is given by: $\nabla = i \cdot \partial/\partial x + j \cdot \partial/\partial y + k \cdot \partial/\partial z = 0$), $\alpha = k/\rho c_P$ [m^2/s] is the thermal diffusivity of the material being inspected, k [W/mK] its thermal conductivity, ρ [kg/m^3] its density and c_P [J/kgK] its specific heat at constant pressure.
The 1D solution of the Fourier equation for the propagation of a *Dirac* heat pulse, that is, an ideal waveform defined as an intense unit-area pulse of so brief duration that no measuring equipment is

capable of distinguishing it from even shorter pulses [10], in a semi-infinite homogeneous and isotropic solid by conduction has the form [9]:

$$T(z,t) = T_0 + \frac{Q}{e\sqrt{\pi \cdot t}} \exp(-\frac{z^2}{4\alpha t}) \tag{7}$$

where Q [J/m^2] is the energy absorbed by the surface, T_0 [K] is the initial temperature and $e=(k\rho c_P)^{1/2}$ [m] is the effusivity, which is a thermal property that measures the material ability to exchange heat with its surroundings

A Dirac heat pulse is composed of periodic waves at *all* frequencies and amplitudes. It is not possible to reproduce such a waveform in practice, a heat pulse provided by a powerful source such as a photographic flash have *approximately* a square shape. In this case, the signal is composed of periodic waves at *several* frequencies. The shorter the pulse, the broader the range of frequencies. At the surface (z=0 mm), Eq. (7) can be rewritten as follows [9]:

$$T(0,t) = T_0 + \frac{Q}{e\sqrt{\pi \cdot t}} \tag{8}$$

Although Eq. (8) is only an approximation of the complex 3D diffusion problem described by Fourier's law - Eq. (6) - many of the PT processing techniques have been based on this simplification to perform qualitative and quantitative analysis.

The following paragraph discusses the experimental aspects of data acquisition by PT.

4.2 Data acquisition

Data acquisition in PT is fast and straightforward as illustrated in Figure 3. The specimen surface is submitted to a heat pulse using a high power source such as photographic flashes. As time elapses, the thermal front will travel through the specimen, and the surface temperature will then decrease *uniformly* over time without flaws. On the contrary, subsurface discontinuities, such as porosity, delaminations, disbonds, fibre breakage, inclusions, etc., can be thought of as resistances to heat flow that produce abnormal temperature patterns at the surface, the thermal changes can be detected with an infrared camera and recorded for later analysis. A synchronization unit is needed to control the time between the launch of the thermal pulse and the recording. Data is stored as a 3D matrix where x and y are the spatial coordinates, and t is the time. Temperature decreases approximately as $t^{1/2}$ (at least at early times), as predicted by Eq. (8), except for the defective areas, where the cooling rate is different. Once the data is acquired, it is available for qualitative and quantitative analysis.

The following sections present two processing techniques that are use in this study.

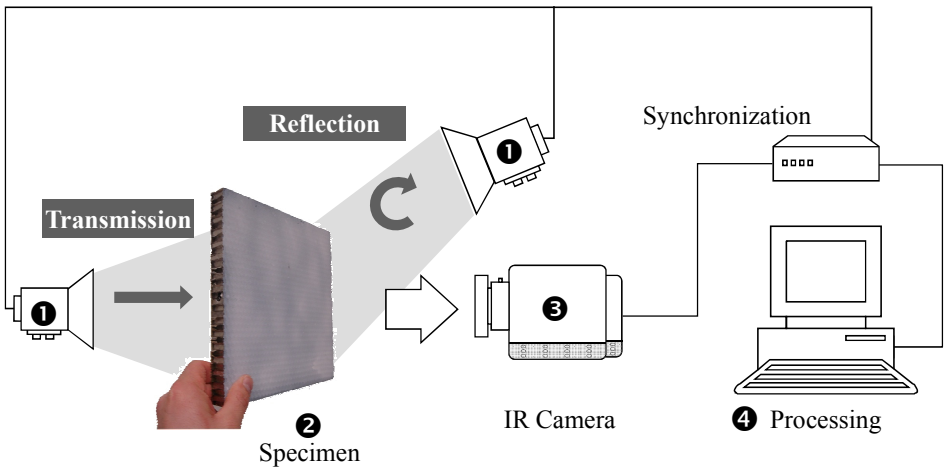

Figure 3. Experimental setup in pulsed thermography.

4.3 Pulsed phase thermography (PPT)

In pulsed phase thermography (PPT) [11, 12], data is transformed from the time domain to the frequency spectra using the one-dimensional discrete Fourier transform (DFT):

$$F_n = \Delta t \sum_{k=0}^{N-1} T(k\Delta t)\exp^{(-j2\pi nk/N)} = \mathrm{Re}_n + j\,\mathrm{Im}_n \tag{9}$$

where j is the imaginary number (j^2=-1), n designates the frequency increment (n=0,1,…N), Δt is the sampling interval, and *Re* and *Im* are the real and the imaginary parts of the transform, respectively.
Real and imaginary parts of the complex transform are used to estimate the amplitude A, and the phase ϕ:

$$A_n = \sqrt{\mathrm{Re}_n^2 + \mathrm{Im}_n^2} \tag{10}$$

$$\phi_n = \tan^{-1}\left(\frac{\mathrm{Im}_n}{\mathrm{Re}_n}\right) \tag{11}$$

Although very useful, Eq. (9) is slow. Fortunately, the fast Fourier transform (FFT) algorithm is available to be implemented or can be found (integrally or simplified) in common software packages.
The phase, Eq. (11), is of particular interest in NDE given that it is less affected than raw thermal data by environmental reflections, emissivity variations, non-uniform heating, and surface geometry and orientation. These phase characteristics are very attractive not only for qualitative inspections but also for quantitative characterization of materials. For instance, a depth inversion technique using the phase from PPT has been proposed [13].

4.3 Principal component thermography (PCT)

As previously explained, the Fourier transform provides a valuable tool to convert the signal from the *temperature-time* space to a *phase-frequency* space but it does so through the use of sinusoidal *basis functions*, which may not be the best choice for representing transient signals such as the temperature profiles typically found in pulsed thermography. Singular value decomposition (SVD) is an alternative tool to extract spatial and temporal data from a matrix in a compact or simplified manner. Instead of relying on a basis function, SVD is an eigenvector-based transform that forms an *orthonormal* space. SVD is close to principal component analysis (PCA) with the difference that SVD simultaneously provides the PCAs in both row and column spaces.
The SVD of an *MxN* matrix **A** (*M*>*N*) can be calculated as follows [14]:

$$\mathbf{A}=\mathbf{U}\mathbf{R}\mathbf{V}^{\mathrm{T}} \tag{12}$$

where **U** is a *MxN* orthogonal matrix, **R** being a diagonal *NxN* matrix (with singular values of **A** present in the diagonal), $\mathbf{V}^{\mathrm{T}}$ is the transpose of an *NxN* orthogonal matrix (characteristic time).
Hence, in order to apply the SVD to thermographic data, the 3D thermogram matrix representing time and spatial variations has to be reorganised as a 2D *MxN* matrix **A**. This can be done by rearranging the thermograms for every time as columns in **A**, in such a way that time variations will occur column-wise while spatial variations will occur row-wise. Under this configuration, the columns of **U** represent a set of orthogonal statistical modes known as empirical orthogonal

functions (EOF) that describes spatial variations of data [15]. On the other hand, the principal components (PCs), which represent time variations, are arranged row-wise in matrix $\mathbf{V}^T$. The first EOF will represent the most characteristic variability of the data; the second EOF will contain the second most important variability, and so on. Usually, original data can be adequately represented with only a few EOFs. Typically, a 1000 thermogram sequence can be replaced by 10 or less EOFs.

5. Acousto – Ultrasonics (AU)

The AU technique attempts to quantify damage in composite materials. The fundamental idea of the AU technique involves the ultrasonic excitation (through a special piezo-ceramic transducer) at a selected / known point upon the material surface and the reception (with a similar type transducer) of the resulting transient elastic waves at another spot on the material surface. A pulsing transducer introduces broadband (Dirac type pulses) ultrasonic waves into the tested sample. These waves propagate along the specimen length to the receiver transducer. The following paragraph discusses the experimental aspects of data acquisition by AU regarding our specimen.

5.1 Data acquisition

During the acousto-ultrasonic (AU) tests one WD type broadband transducer was used as a pulser and one pico transducer also broadband was used as a receiver. Both are manufactured by PAC (Physical Acoustics Corporation USA) and provided by Envirocoustics (Greece).
The transducers were placed upon the specimen with special clamps at the specified distance of 50 mm for each AU measurement. The acquisition board was a 16-bit PCI-2 by PAC. Pre-amplification of 40 dB and band-pass filtering at 20-1200 kHz was performed by 2/4/6-AST preamplifiers also manufactured by PAC. Δt front end filtering excluded recordings out of the gauge length. The recording parameters PDT, HDT and HLT were set to the following values: PDT= 50 μsec, HDT= 200 μsec, HLT=800 μsec, whereas the recording threshold was set at 40 dB.

6. Comparative results

The experimental arrangement, used to record holographic interferograms was a typical holographic system, as the one shown in Figure 2 [16]. A continuous-wave laser (λ = 532 nm) of 250 mW power was employed as the source of coherent light.
Holographic interferograms were recorded under two different modes of stressing viz., thermal loading by a welder (P_{max} = 400 W) positioned in transmission mode and forced convection.
Stressing by a welder has been proposed also recently on another sandwich structure [17].
The most effective stressing to obtain the information along the thickness of a component is established as transient thermal stressing. The method and extent of stressing depends on the material property, geometry, and dimensions of the sample. Uniformity in stressing is very important during heating [18]. To take into consideration the complexity of the sample, two different stressing methods and two holographic interferometry techniques (DE and RT) have been selected. The sample was carefully prepared in order to produce inclusions and detached region for reference purposes.
In the first analysis with the DE technique, interferograms were recorded after the sample had been heated by a welder on honeycomb surface (Figure 1a); the surface temperature rose to about 180 °C, although the day before the sample was kept to about – 20 °C in a freezer. Between the exposures the object has been cooled in air.
For a stressed zone of the object without surface geometrical discontinuities, distortions of the fringes indicate abnormal surface deformation and, consequently, the presence of some internal defects.
Figure 4a shows the trend of the holographic fringes for the sample cooled in air (t_{exp} = 0.9 s, t_{fti} = 3s). As can be seen, the trend of fringe pattern is regular to the left, but to the right there is a

bending relatively to the defect C and with greater evidence for the defect D; therefore, the presence of defects is indicated by discontinuities in the fringe system, but the exact outline of the defects cannot be discerned.

By varying the cooling period, the surface temperature of the second exposure changes and consequently, the fringe number varies. In particular, a decrease in temperature change causes a reduction in the number of fringes; in fact, by increasing the time interval between the exposures (t_{exp} = 0.9 s, t_{fti} = 5 s) in order to reach a greater temperature change, the fringe pattern of Figure 4b is obtained. The trend of the fringes is the same, but their marked distortions show more clearly the position and extension of the defect D. With this method, we have not found evidence about defect A, probably due to the different stopper inserted in the defect C in comparison to defect A (Figure 1c), with different repercussion on the heat transmission and therefore on the detectable perturbations in the surface deformation. Besides, the Teflon layer that covers the inserted sponge in defect A, is slightly thicker than the layer that covers the inserted sponge of defect C.

On the other hand, defect B appears in the second experiment. RT technique (t_{exp} = 1 s) and the heating forced convection have been used in this case. Two experimental results recorded at different times of cooling have been reported (Figure 4c and Figure 4d). From Figures 4c and 4d can be observed that the fringe patterns kept their uniformity, except over the defect D.

Presumably, the cycles of heating and cooling used, a precedent weakness point of the material and a low resistance of the material to important thermal shocks, have produced this real defect inherent the ceramic material.

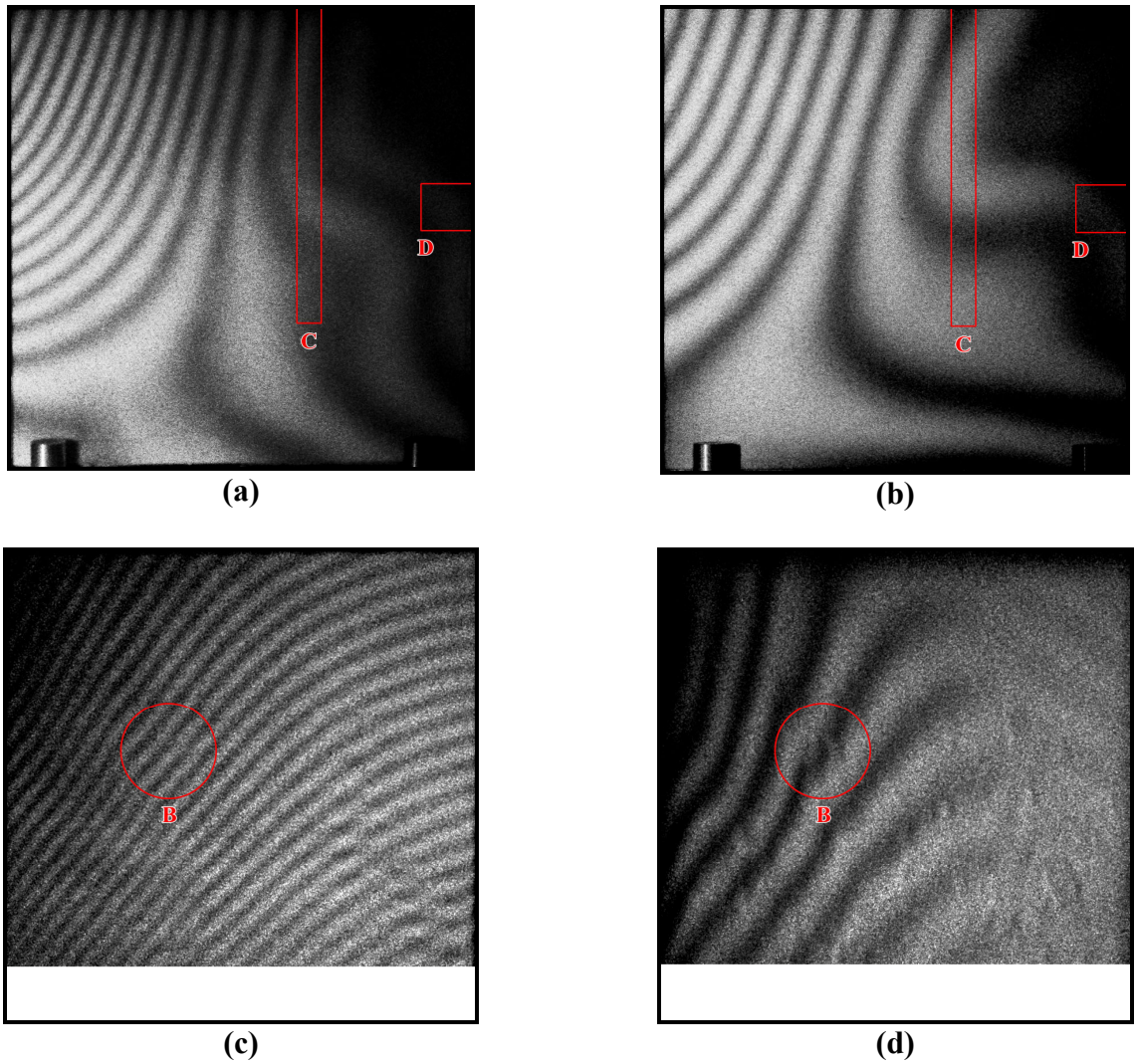

Figure 4. (a) Fringe pattern of a defective sample, thermally stressed at ≈ 200 °C and cooling in air for 3 s, (b) Fringe pattern of a defective sample, themally stressed at ≈ 200 °C and cooling in air for 5 s, (c) RT result of the defect B , (d) another RT result of the defect B .

Figure 5 presents some results obtained by pulsed thermography in both reflection and transmission modes.
Figure 5a shows a phasegram obtained after processing data from a reflection mode experiment using two photographic flashes. As can be observed, only defect D can be identified.

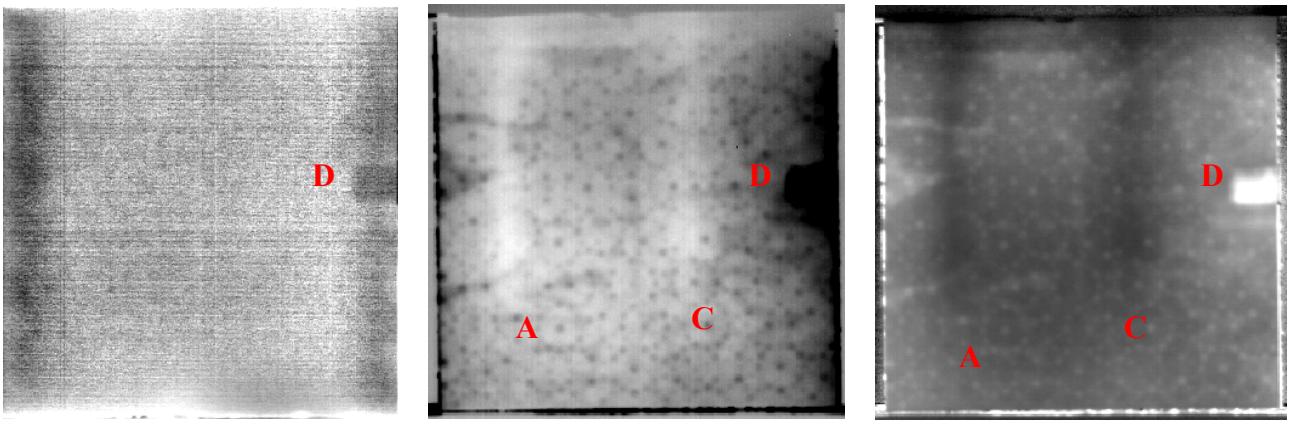

(a) **(b)** **(c)**

Figure 5. PT results: (a) PPT phasegram f=0.02 Hz from reflection mode, (b) third empirical orthogonal function by PCT in transmission mode, and (c) PPT phasegram at f=0.014 Hz in transmission mode.

The specimen was also inspected in transmission mode heating for 1 minute with two halogen lamps and data was processed by PCT and PPT. The third empirical orthogonal function obtained by PCT is presented in Figure 5b. In this case, defects A, C and D are detected. The honeycomb structure can also be seen. A PPT result is shown in Figure 5c, in which the same features can be seen.
From these results can be observed that this kind of specimen is more easily inspected in transmission mode.
Preliminary tests performed in reflection mode using halogen lamps with different heating times show no defect detectability improvements with respect to the results obtained using the photographic flashes (Figure 5a). From experimental analysis varying the heating time of the halogen lamps in transmission mode, it can be thought that similar results as those presented in Figure 5b and Figure 5c could be obtained using the flashes in transmission mode (although not tested at this time).
Much more energy would be required in reflection mode in order to be able to detect defects A and C and to improve contrast of defect D.
This is mainly due to the thermal properties of the ceramic material that acts as a resistance to the thermal front. In reflection mode, heat propagates from the surface to the defects locations and then it travels back to the specimen surface. The situation is different in transmission mode. Here, heat travels from the rear surface to the front, considerably reducing the energy requirements for defect detection.
Defect B was not detected both by pulsed thermography as can be seen from Figure 5 that by AU technique.
The latter technique was conducted to identify and confirm the defects found by the techniques previously described.
For the assessment of defects A and C in comparison with the healthy state the measurements were conducted as shown in Figure 6.
In all three cases the two sensors were put 50 mm apart.
In each position at least 15 AU waveforms were recorded. The differentiation of each defect with the undamaged region is quantified after the extraction of several characteristic parameters from the AU signals.
Energy, signal strength, counts, duration are only a few.

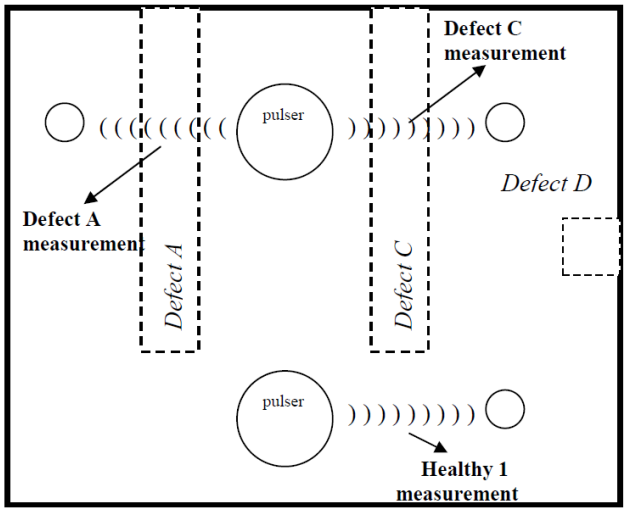

Figure 6. Sensor placement for defects A and C assessment

Statistical analysis and calculation of the mean values of the above mentioned parameters was necessary. Figure 7 shows the differentiation in signal strength and counts to peak.

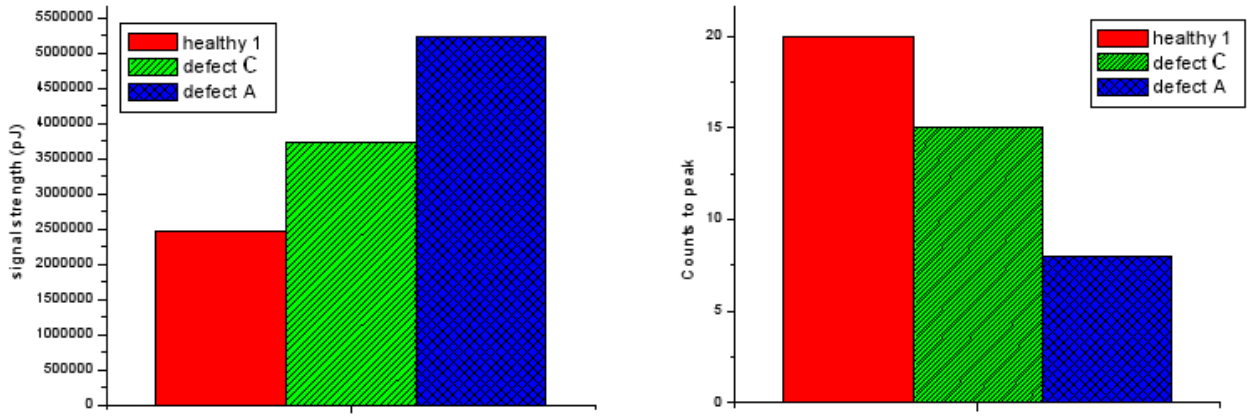

Figure 7. Signal strength and counts to peak as extracted from AU waveforms for defects A and C as compared with the healthy state

For the assessment of defect D in comparison with the healthy state the measurements were conducted the way Figure 8 depicts.

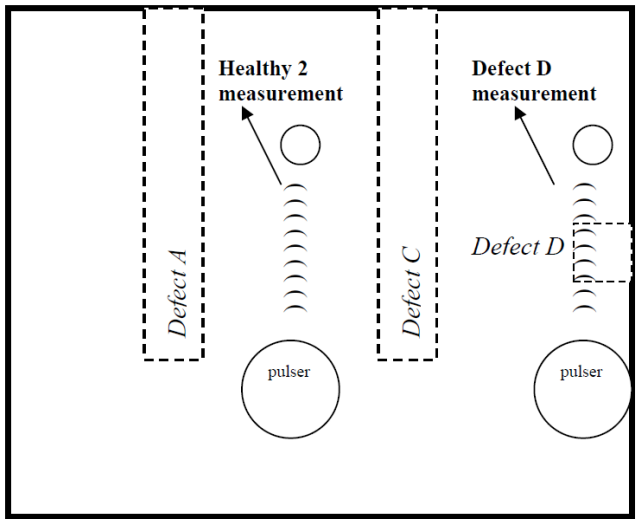

Figure 8. Sensor placement for defect D assessment

In Figure 9 the differentiation in signal strength and counts to peak are shown.

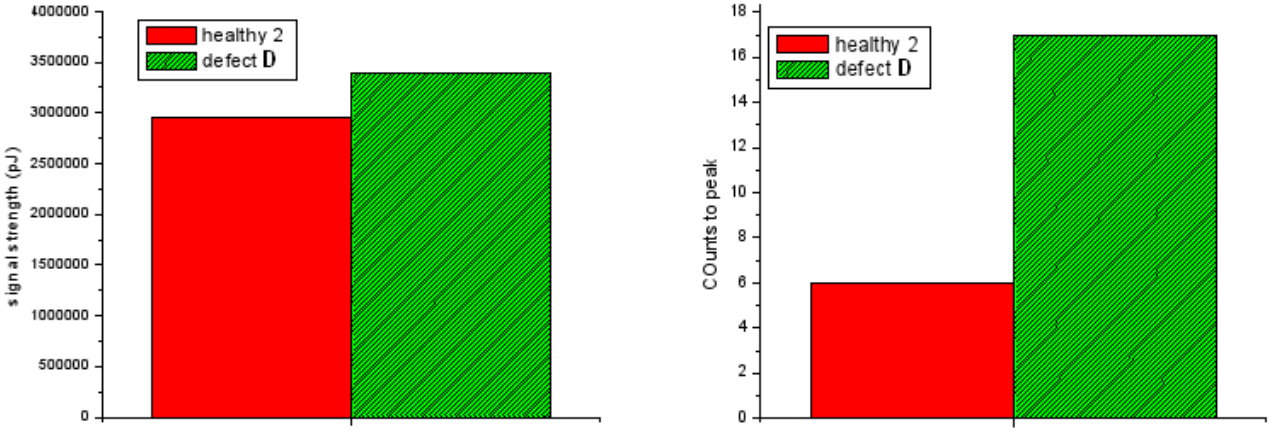

Figure 9. Signal strenght and counts to peak as extracted from AU waveforms for defect D as compared with the healthy state

7. Conclusions

HI, IRT and AU are well suited for the NDT of complex sandwich structure with bonded alumina layer.
Considering the typical defects gravity for composite structures, these techniques confirm the importance of the integration and the application on such materials, with the purpose to identify the greatest number of present defects.
It was possible to detect perforated honeycomb cells φ = 5 mm in diameter with inclusions of two sponges covered by Teflon (defects A and C) with IRT and AU techniques. HI method, in the DE technique, only confirms the defect C presence, probably because the two sponges are covered by Teflon layers of different thickness, resulting of different elasticity when subjected to a thermal loading. This fact combined with the different stopper used for defects A and C (as seen in Figure 1c) can have resulted on the detectable perturbations in the surface deformation.
RT technique provided an interesting result for the defect B: the holographic results presented in Figure 4c and 4d suggest that this defect is inherent the ceramic material. The thermal signature of defect B (Figure 5) is apparently similar to the rest of the ceramic, so it is not detected by PT. At the same time, HI is able to detect defect B but, as mentioned, not defect A, the latter being detected by PT in transmission mode. Defect D - detach region - is confirmed with great evidence by the three techniques used in this work.
The use of another NDT in order to confirm the presence of the defect B as the use of Sandwich Holography (SH) for the identification of the defect A are two possible developments of this integration. All these considerations provide a hint of the complementarity of these three techniques for the NDT of materials.

Acknowledgments

We wish to thank P. Montanari, F. Pastorelli and M. Tursini of Thales Alenia Space – L'Aquila – for to have furnished us the ceramic plate in alumina and the sandwich structure with the relative technical characteristics.

References

1. T.A. Taylor, C.G. Bergeron and R.A. Eppler, *Ceramic coatings*. In Metals Handbook, 9th edn, Vol. 5, T.B. Zorc, Metals Park, OH, 1982, pp. 532 – 547.

2. D.W. Richerson, *Modern ceramic engineering. Properties, processing and use in design*, ISBN 0 8247 8634 3, Marcel Dekker Inc., 1992, 860 p.
3. A.G. King, *Ceramic technology and processing*, ISBN 0 8155 1443 3, William Andrew publishing, 2002, 512 p.
4. United States, Patent Application publication, *Pub. No. US 2004/0113863 A1*, June 2004.
5. M. Horman, Appl. Opt. **4**, 1965, p. 333.
6. K.A. Stetson and R.L. Powell, *Hologram Interferometry*, J. Opt. Soc. A. **56**, 1966, pp. 1161 – 1163.
7. H.K. Liu and R.L. Kurtz, *Thermal loading in the laser holography non-destructive testing of a composite structure*, NASA TR R-439, National aeronautics and space administration, Whashington, D.C., May 1975.
8. P.C. Mehta and V.V. Rampal, *Lasers and holography*, World Scientific 1993, ISBN 981 02 1214 3, p. 681.
9. H. S. Carslaw. and J. C. Jaeger. *Conduction of Heat in Solids*, 2nd edition, Clarendon Press, Oxford (1986).
10. R. Bracewell. The Fourier Transform and its Applications, McGraw-Hill, USA (1965).
11. Maldague X. P. and Marinetti S. "Pulse Phase Infrared Thermography," *J. Appl. Phys.*, **79**(5):2694-2698, 1996.
12. Ibarra-Castanedo C. and Maldague X. "Pulsed Phase Thermography Reviewed," *QIRT J.*, **1**(1):47-70, 2004.
13. Ibarra-Castanedo C. "Quantitative subsurface defect evaluation by pulsed phase thermography: depth retrieval with the phase," *Ph. D. thesis*, Laval University, 2005. [accessible online: http://www.theses.ulaval.ca/2005/23016/23016.pdf].
14. Rajic N. "Principal component thermography for flaw contrast enhancement and flaw depth characterization in composite structures," *Compos. Struct.*, **58**:521-528, 2002.
15. Marinetti S., Grinzato E., Bison P. G., Bozzi E., Chimenti M., Pieri G. and Salvetti O. "Statistical analysis of IR thermographic sequences by PCA," *Infrared Phys. & Technol.*, **46**:85-91, 2004.
16. A. Di Ilio, A. Paoletti and D. Paoletti, *Holographic tests on ceramic coatings on metal surfaces*, Short Communication, Composites Science and Technology **57**, 1997, pp. 365 – 369.
17. S. Sfarra, C. Ibarra-Castanedo, N.P. Advelidis, D. Kourousis, A. Anastassopoulos, A. Bendada, X, Maldague, D. Ambrosini, D. Paoletti, *A comparative investigation for the nondestructive testing of honeycomb structures by holographic interferometry and infrared thermography*, ICPPP'15, 15th International Conference on Photoacoustic and Photothermal Phenomena, Leuven, Belgique, 19-23 July 2009.
18. B.P. Thomas, K.V. Rajendram and S.A. Pillai, *Wholefield NDT of Porous Materials Using Digital Holography*, Proc. National Seminar on Non-Destructive Evaluation, 2006, Hyderabad.